CONTAINMENT SCALING: EXPERIMENTAL INVESTIGATION OF THE BREAK-UP OF A STRATIFIED LAYER DUE TO A VERTICAL JET FROM BELOW

M. Ritterath¹, R. Heierli¹, G. Mignot² and H.-M. Prasser¹

Swiss Federal Institute of Technology (ETH), Zurich, Switzerland ritterath@lke.mavt.ethz.ch, prasser@lke.mavt.ethz.ch

Paul Scherrer Institute, Villigen, Switzerland guillaume.mignot@psi.ch

Abstract

In the context of containment safety, the break-up of a helium (helium as substitute for hydrogen) layer due to an upward vertical jet in a confined volume was the subject of experimental investigation in two geometrically similar test facilities scaled 1:4. The high instrumentation resolution in space and time of the small-scale facility (MiniPanda) provided 2D temperature field and 1D helium concentration profile measurements well suited for CFD validation and detailed analysis of the break-up process. In order to conduct similar experiments on the scaled facilities, the boundary conditions (i.e., the jet diameter and velocity) for the experiments with two length scales have been scaled with regard to a Froude number relating the jet's buoyancy to the jets inertia at the helium layer interface. The different flow phenomena observed in the two facilities are discussed based on experimental results.

1. Introduction

For assessment of light water reactor containment safety after a severe accident, both, experimental and analytical investigations of phenomena involved must be considered. Because of the huge dimensions of commercial light water reactor containments, test facilities are scaled down to make experimental studies feasible. Scaling laws are required in order to transfer the learnings from the model to the real containment. Uncertainties due to scaling distortions can only be estimated, because not all dimensionless similarity numbers that describe the flow field can be kept constant during the scaling. An experimental verification of the scaling is usually not possible, since full scale data is mostly unavailable. Issues with scaling experiments to real containment size were subject to theoretical investigations in the past. Possible scaling approaches were proposed and discussed in many publications (Karwat 1987; Peterson 1994; Wulff 1996; Peterson, Schrock et al. 1998; Zuber, Wilson et al. 1998; Revankar, Oh et al. 2009; D'Auria and Galassi 2010). The importance of containment experiment scaling is highlighted by the fact that a project, "Scacex", in the frame of the 5th Euroatome Framework Program, was dedicated to scaling of containment experiments (Fischer, Wolf et al. 2002). Still, no completely straight-forward method to derive scaling laws has been found. However, a scaling methodology was proposed that includes a system/phenomena decomposition in order to identify the governing processes. This requires an understanding of the process and introduces a degree of user dependency. The equations describing the main processes are than scaled to meet the experimental limitations (e.g., size of test facility or electrical power required for the experiment).

The experimental results obtained from scaled-down test facilities are used to assess the ability of simulation codes to predict the correct thermal-hydraulic system response for different accident scenarios. The need for a high quality database of experimental data dedicated to the transport of hydrogen has been identified (Yadigaroglu, Andreani et al. 2003). The break-up of an already stratified hydrogen layer in the upper part of the containment was found to especially challenge the simulation codes during the ISP 47 exercise (Allelein, Fischer et al. 2007). The hydrogen issue originates from hydrogen that can be generated after a loss of coolant accident and a failure of all residual heat removal systems. Due to an insufficient decay heat removal from the fuel cladding (zirconium alloy), hydrogen is formed by the oxidation of Zirconium with water. In the consequence of the hydrogen release from the core, a major phenomenon threatening the integrity of the containment is the accumulation and transport of hydrogen which could potentially deflagrate when exceeding a critical concentration.

To the current state of knowledge, in Fukushima, Japan, hydrogen was formed after the decay heat removal failed. A mixture of hydrogen and steam was vented into the torus (wetwell) in order to depressurize the reactor pressure vessel. Since the torus cooling was not available either, the pressure increased in the primary containment (drywell). The Mark-I containment is inertialized with nitrogen in order to mitigate the risk of hydrogen explosion inside. To the current state of knowledge it is assumed that, when venting the containment to relief the pressure, hydrogen escaped from this inert environment into the reactor building. The consequent transport processes play an important role on the hydrogen distribution and on the consequent mechanical load originating from the hydrogen explosion.

PANDA is a large-scale containment test facility at the Paul Scherrer Institute, Switzerland. There, experiments have been carried out in the frame of the OECD/NEA SETH-2 project to contribute to a database for phenomena related to the safety of light water reactor containments and the hydrogen transport (Dreier, Paladino et al. 2008).

While course mesh lumped parameter (LP) codes such as GOTHIC are able to cope with true size containment models, for CFD codes true size containment studies are still computationally very expensive due to the fine meshes required (and the mesh variation studies). Consequently, the data of large-scale test facilities are only rarely used to assess modern CFD codes such CFX, StarCCM+, or FLUENT. Furthermore, the spatially coarse instrumentation of the large scale test facilities compared to the cell size of the CFD meshes allows only for comparison of integral quantities.

A small-scale containment test facility, named MiniPanda, has been built at ETH Zürich in order

- to provide experimental data of phenomenon related to the safety of nuclear reactor containments highly resolved in space and time and in order
- to allow for the experimental investigation of scaling effects by conducting experiments on two different scales.

It was designed by uniformly scaling down the upper two out of four main vessels ("drywells")

from the PANDA facility by factor of 1:4. MiniPanda was equipped with novel and dense instrumentation to support the development and verification of codes, both CFD and LP.

A layer break-up experiment carried out at MISTRA containment test facility (Saclay, France) was compared to a similar experiment at PANDA (Villigen, Switzerland). In both large-scale thermal-hydraulics test facilities with a vessel height of about 8 m, a helium rich cloud was created in the upper quarter of the vessel during the pre-conditioning phase. An eccentrically vertical upward air jet impinged on - and eroded the layer during the test. For these two experimental series, a non-dimensional number, similar to a Froude number, was defined in order to compare to the experimental results obtained with the two facilities (Studer, Brinster et al. 2010):

$$Fr_2 = \frac{U}{\sqrt{g \cdot \frac{(\rho_{air} - \rho_s)}{\rho_{air}} \cdot h_{layer}}}$$
 (1)

with U as the assumed velocity of the jet at the layer interface, g gravity constant, h the thickness of the helium-rich layer and ρ_{air} and ρ_{S} the densities of the air and the layer, respectively. This Froude number was based on ideal initial test condition and changed during the duration of the test. For this comparison, the time axis was scaled in order to compensate for different volumes of the helium-rich layers and different injection flow rates by a residence time, t_{air} :

$$t_{air} = \frac{V_{cloud}}{Q_{v,air}} \tag{2}$$

where $V_{\rm cloud}$ is the volume of injected helium and $Q_{\rm (v, air)}$ is the volumetric flow rate of injected air. Studer et al. found a good agreement in the comparison of the helium concentration evolution for sensors at corresponding positions in PANDA and MISTRA facility for experiments with a similar Fr_2 number (i.e., ST1 7, PANDA and LOWMA4, MISTRA).

In the following sections, first the small-scale test facility and its instrumentation are described. Second, the small-scale experiment's specifications, that are aimed to be similar to the large scale experiments specifications are presented together with the applied scaling. Finally, the evolution of the layer break-up in MiniPanda and its scalability to the PANDA experiments are discussed.

2. Facility and instrumentation description

MiniPanda is geometrically similar to the upper two vessels of PANDA (drywells), scaled down in size by a factor of 4.17 and consists of two vertical cylindrical vessels, each 1 m in diameter and 2 m high. These two vessels are interconnected by means of a 1340 mm long horizontal pipe, inner diameter 220 mm, with a 70° bend of radius 170 mm after half of the pipe length. The vessel shells (wall thickness 16 mm), top and bottom lids (wall thickness 10 mm) and the pipe (wall thickness 2.5 mm) are made from PVC(-U). The operation is limited to atmospheric pressure and temperature regimes, so that the inner wall temperature does not exceed 70°C (peak temperature up to 200°C).

One vessel, referred to as Vessel 2, is equipped with a vertical injection line (aluminum, ID=18 mm, OD=19 mm, exit 1000 mm above ground on and 125 mm away from the wall, see Figure 1). Inside the injection pipe, a heater wire helix with adjustable power is installed allowing for heat-up of the injected air flow.

The facility was equipped with off-the-shelf instrumentation such as

- eight 1 mm mantle thermocouples, type K, four on each vessel axis,
- three pairs of inside and outside wall thermocouples (6 k-type mantle TC) and
- forty-five katharometer ("g", see Figure 1) helium sensors to measure the gas composition distribution. The katharometers were distributed on key positions important for the experiment, mostly in the upper part of Vessel 2 (vertical distance between the katharometer levels 50-100 mm). The katharometers' time constant was estimated to be 1 s.

Furthermore, MiniPanda was equipped with new temperature mesh sensors, which read the temperature from 780 NTC-thermistors (time resolution 0.8 s, compare Nureth14, Log: 441). These thermistors were mounted in between the crossing points of two coplanar wire planes that are not touching each other. The measurement principle is based on the wire mesh principle introduced by Prasser et al (Prasser, Böttger et al. 1998), which scans line-wise the local conductivity between the transmitter (wire of the first plane) and the receiver (wire of the second plane). The temperature measurement matrix was spatially distributed on 5 planes:

- Two horizontal temperature mesh sensors covered the horizontal cross-section of Vessel 2 at elevation 1135 and 1673 mm ("b" and "c", Figure 1). The spatial pitch of this sensor matrix was 57 mm.
- One horizontal temperature mesh sensor (175x175 mm²) spanned 500 mm above and concentrically with the exit of the injection pipe (elevation 1500 mm, pitch 25 mm, "e", see Figure 1).
- Another temperature mesh sensor was arranged vertically inside the interconnecting pipe (pitch 25 mm, not shown).
- The last temperature mesh sensor covered the vertical symmetry plane of Vessel 2 (defined by vessel axis and center point of interconnecting pipe, including the injection line) from elevation 1135 mm until 1923 mm (horizontal pitch 57 mm, vertical pitch 30 mm) ("d", see Figure 1).

In addition, MiniPanda was equipped with four in-house developed pulsed-wire anemometers (Ritterath, Voser et al. 2009), "a", see Figure 1, in the interconnecting pipe and 8 pairs of ultrasound transducers for high-speed (3 Hz) helium fraction measurement (Ritterath, Prasser et al. 2010).

Figure 1 depicts the geometry of MiniPanda and the sensor locations.

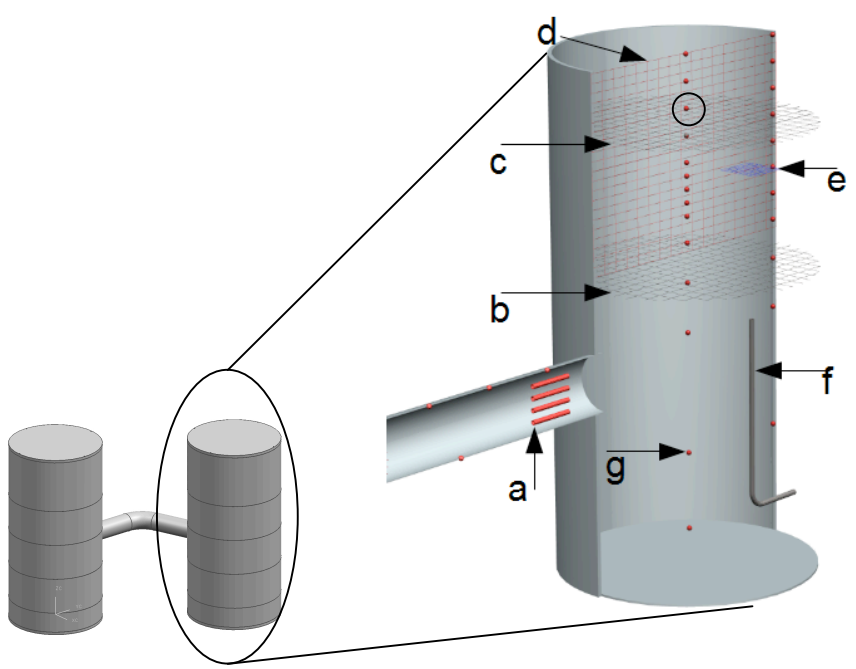


Figure 1: Schematic of MiniPanda and a detailed view of Vessel 2 and its instrumentation.

3. Experiment specification

The small(/smart)-scale experiments were carried out at room temperature and at ambient pressure, similar to the experiments of the large-scale facility. During the preconditioning phase, a helium-rich layer with a nominal concentration of c_0 was formed by injecting a helium-air-mixture with the corresponding concentration from the top of the vessel. The injected volume of 367 1 corresponded to a nominal layer thickness of 0.5 m. In fact, the vertical helium concentration showed a transition region of about 0.3 m (10-90% \cdot c_0) between the higher region of the vessel, with the nominal helium concentration, and the lower part of the vessel with zero helium concentration (see Figure 3 in section 4). Anyway, the initial vertical helium profile could be well-reproduced for all tests, as can be seen from Figure 3a where the initial helium profile are the same for both tests.

The test started with the beginning of the air flow through the injection line. The flow rate was controlled by a Red-y GSC mass flow controller with maximum 1.5% flow rate uncertainty. The heater was activated together with the mass flow controller, increasing the temperature of the injected air to 85°C (measured with a thermocouple in the injection line). On the top of the other vessel, a 22 mm vent hole was permanently open to allow for pressure equilibration. It took for experiment MPII_1 about 2200 s until the layer was eroded and homogeneous helium concentration in Vessel 2. After this break-up, the well mixed helium concentration decreased according to the dilution by the continuously injected air.

In order to provide comparability between the layer erosion process of the small-scale and the large-scale facility, an interaction Froude number was defined. The interaction Froude number relates the nominal initial conditions of the inertia to the buoyancy of the jet inducing the layer break-up, see Eq. (3), and considers the jet diameter, d_{int} , as a length scale (compare Eq. (1))

$$Fr_{\text{int}} = \frac{u_{\text{int}}}{\sqrt{g \cdot d_{\text{int}} \cdot \frac{(\rho_0 - \rho_{\text{int}})}{\rho_0}}}$$
(3)

where u_{int} is the estimated jet velocity at the interface, d_{int} the estimated jet diameter at the interface, ρ_0 is the density of the injected fluid, and ρ_{int} the density of the helium layer. These values describe nominal initial conditions. The velocity, u_{int} , and the diameter, d_{int} , at the interface were computed according to the expansion of a free jet (Schlichting 1960):

$$\frac{u_{\rm int}}{u_0} = \frac{13.14}{4.39 + x/r_0} \tag{4}$$

with x, the distance from the source and r_0 the efflux diameter.

$$\frac{D_{\text{int}}}{D_0} = 0.848 \cdot (4.39 + x/r_0) \tag{5}$$

The Froude number was adjusted by varying the injected flow or the helium concentration of the layer. Table 1 summarizes the key parameters of the experiments. The Reynolds number at the exit, Re_{exit} , as well as the residence time that scales the time axis, τ_{dil} , are displayed. The diffusion time given in Table 1, τ_{dif} , depends on the initial concentration of the layer and is a measure, how long it takes without jet to reduce the helium concentration in the middle of the layer to half of the original concentration. It will be used later in order to discuss the influence of diffusion to the experiment.

Experiment Flow Length $Fr_{\rm int}$ Fr_2 $Re_{\rm exit}$ c_0 $au_{
m dil}$ $au_{
m dif}$ [mol-% name rate scale [-] [-] [-] [s][s]He] [l/min] MPII 1 100 42.1 0.70 0.24 2350 613 2930 1 MPII 2 2930 100 78.7 1.3 0.45 4400 275 1 MPII 3 100 157 1 0.91 8800 164 2930 2.6 MPII 4 100 54.5 1 0.9 0.31 3000 474 2930 MPII 5 100 18.2 1010 1422 2930 1 0.3 0.11 MPII 6 35 22.3 1 0.80.24 1250 405 4170 ST1 7 40 776 4.17 0.49 14000 806 70000 0.6

Table 1: Key parameters of the experiments.

4. Evolution of layer break-up in MiniPanda

The stratified helium rich layer was confined to the top of Vessel 2. There, it was subject to 1) molecular diffusion and 2) erosion induced by the vertical jet from below.

1) The diffusion was quantified by experiments where the helium-rich layer was left without a jet after preconditioning for initial molar fraction of the layer of 100, 35 and 8% helium. Due to the sharp gradient from the helium-rich to the helium-poor zone, helium diffused rapidly and was

distributed throughout the whole vessel. A simple 1D diffusion simulation with the measured initial vertical helium profile as an initial condition was carried out with a diffusion coefficient of 0.8e-04 m2/s (VDI 2008). The exact agreement between the analytical and the experimental evolution of the helium profile proves the absence of any undesired secondary side-effects such as initial turbulence or initial convections due to filling.

A diffusion time, τ_{dif} , was introduced, describing how long it took to reach 50% of the initial helium fraction at a point 200 mm below the top of the vessel (see Figure 1, katharometer marked with a circle, approximately in the middle height of the initial helium layer). The diffusion times were 2930 s, 4170 s and 5485 s for 100%, 35% and 8% initial molar helium fraction, respectively. Although the definition of τ_{dif} was arbitrary, it proved a strong superposition of diffusion on the flow phenomena observed.

2) The vertical air jet from the near wall injection is slightly buoyant due its higher temperature compared to the temperature of the environmental air. The jet evolved (i.e., the velocity and temperature decay and the jet diameter increases). After about 0.2 m, the jet entered the transition region, where the local density decreased due to the increasing helium fraction. In the light gas environment, the air jet's momentum is dissipated by the negative buoyancy force. The jet stopped its upward motion when all momentum is dissipated at the stagnation point S (see Figure 3, b). From this highest point, the heavier air fell back downwards creating a mushroom-shaped indentation in the temperature field. This impingement of the jet introduced turbulence into the helium layer and enhanced the mixing at the interface between the helium layer and the low-helium environment, and by this erodes the layer. At the same time, helium was washed down into the area below the stagnation point. Figure 2 displays the helium fraction evolution at the top and below the layer. The concentration at the top decreased due to diffusion and to air entrainment. In the zone below the stagnation point, helium fraction increased so that the upper and lower helium fractions approached each other during the experiment progress experiment. The area below the stagnation point (above the interconnecting pipe) is well mixed.

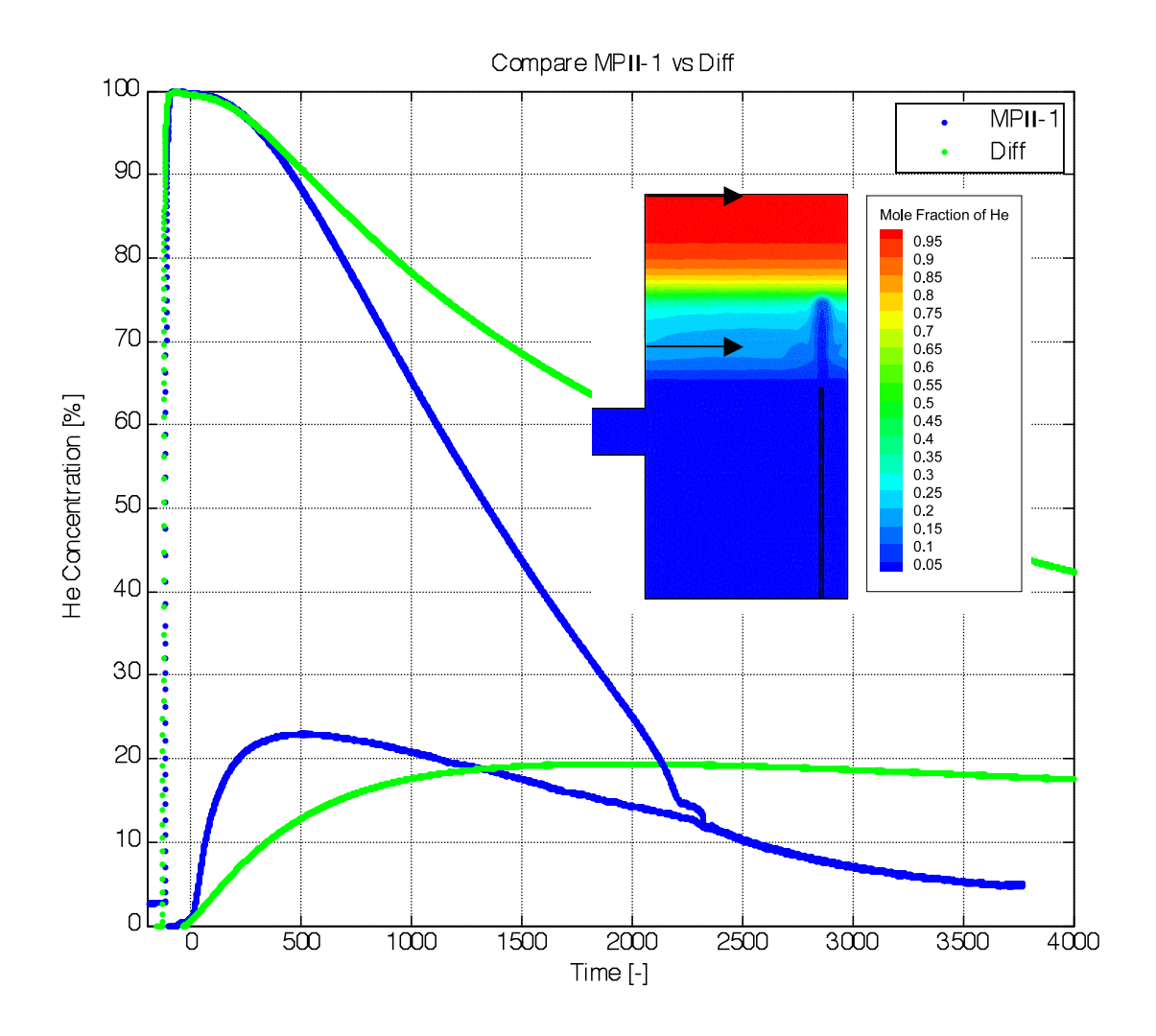


Figure 2: Helium fraction evolution at the top of the vessel and in the zone between the injection the initial layer. The arrows mark the measurement positions. Background picture is the estimated helium fraction distribution after 100 s.

As erosion progressed, the upwards propagating jet faced the very light gas zone only in higher zones, but was more subject to negative buoyancy as soon as it exited the injection pipe. Additionally, the density difference between the jet and the helium layer decreases due to air entrainment into the layer. This leads to an upward motion of the stagnation point, and thus a progression of the layer erosion. However, the jet is not affected by the helium profile above the stagnation point.

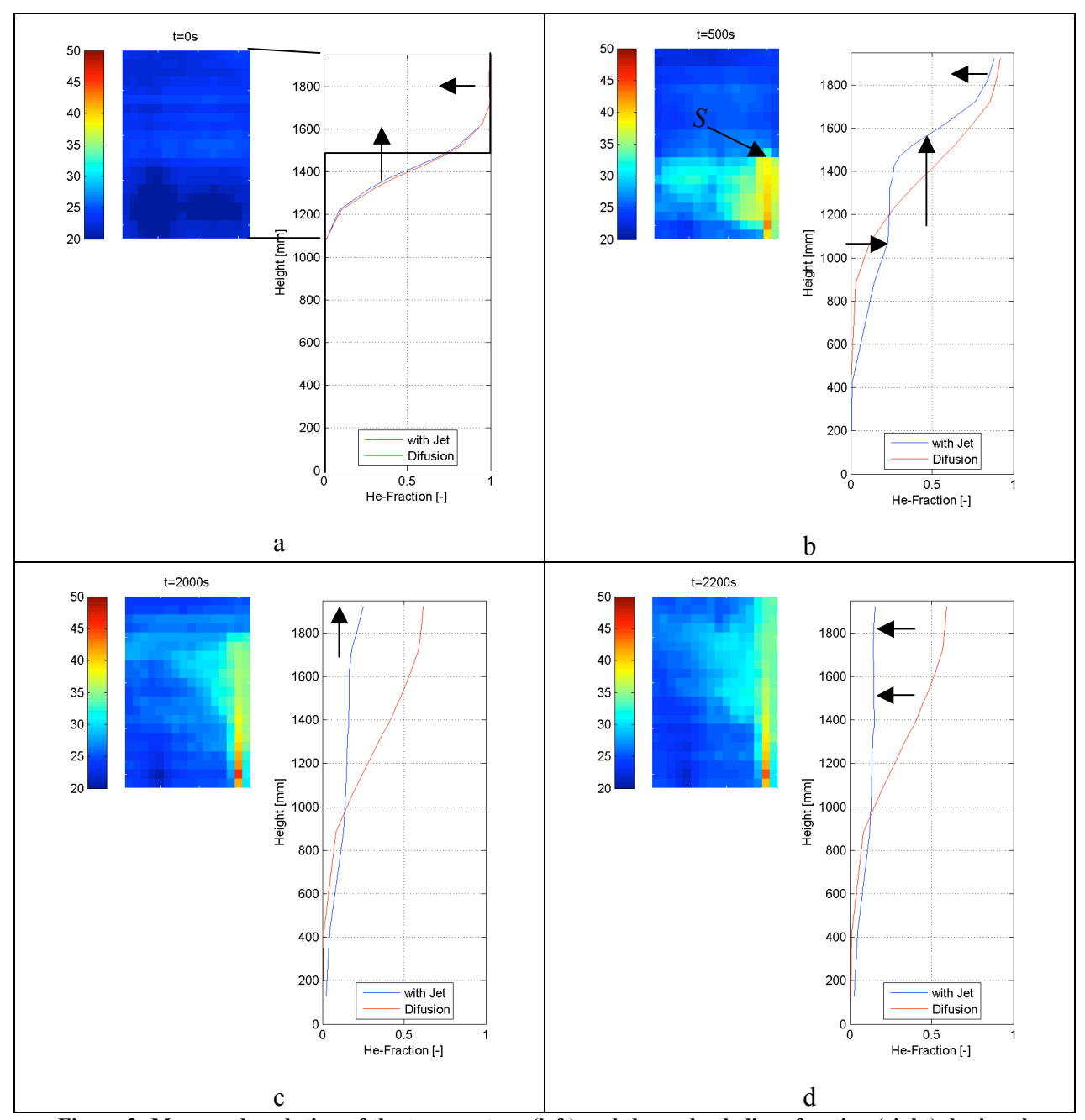


Figure 3: Measured evolution of the temperature (left) and the molar helium fraction (right) during the course of the layer break-up.

Figure 3, "a", displays the initial (*t*=0) vertical helium profile (right) for the experiment with jet (blue) and the one where the helium was left without jet (red). The positions of the measurements are vertically aligned in these graphs. The nominal helium layer is sketched as a black solid line (i.e., 100% helium 1423 mm above the bottom of the vessel). On the left side, the corresponding temperature field is displayed (cold=blue, warm=red).

During the course of the experiment, an upward motion of the stagnation point, S, and an increase of the helium concentration in the lower part of the vessel were observed due to the interaction of the jet with the layer interface (see Figure 3, "b"). At the same time, the concentration of the helium reservoir at the top of the vessel decreased. This decrease was accelerated in the presence of the jet (see Figure 3, "b" and "c": The blue curve (with jet) shows, for the same time, less helium concentration at the top than the red curve (pure diffusion)). In other words, the helium concentration decrease was caused by a superposition of diffusion and turbulence-enhanced mixing. At a height of 910 mm, the upper edge of the pipe connecting the second vessel penetrates into the vessel. There, the helium profiles exhibit a bend because the helium leaves through the pipe towards the other vessel. Figure 4 displays the velocity evolution in the upper (a) and the lower (b) part of the interconnecting pipe that was measured with the highest and the lowest anemometer shown in Figure 1 (a). From the beginning of the experiment on, a vent flow was established through the IP in direction of Vessel1 (vent vessel), firstly covering the whole cross-section of the IP. After about 100 s, a counter-current flow was established (i.e., the sign of the flow in the lower part of the IP changes to negative, see Figure 4 (b)). This counter-current flow set up time was linked to the moment, when the helium fraction of the gas exiting from Vessel 2 increased due to the wash-down from the reservoir (This effect is further discussed in Nureth14, Log: 441).

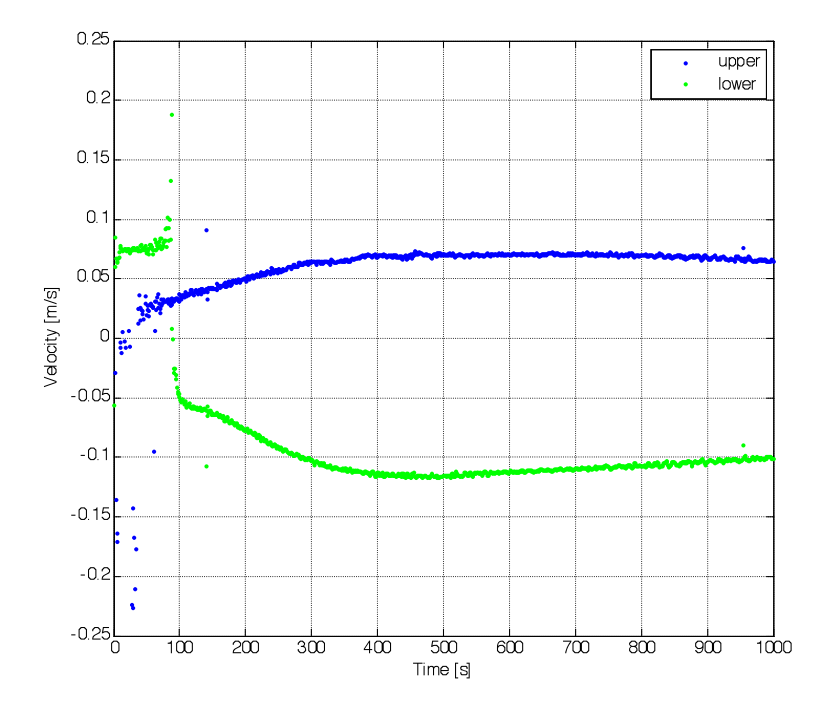


Figure 4: Velocity in the upper (blue) and the lower (green) part of the interconnecting pipe. Positive velocity from Vessel 2 (injection vessel) to Vessel 1 (vent vessel).

The layer break-up was finished when the stagnation point reached the top of the vessel (see Figure 3, "d"). From that moment on, the helium concentration with jet (blue curve) followed a

dilution process. However, even in the absence of the jet, the maximum helium concentration of the reservoir decreased to about 55% of the initial concentration.

Repetition experiments were carried out for MPII_1 and MPII_2. Their results match the original results and prove their validity.

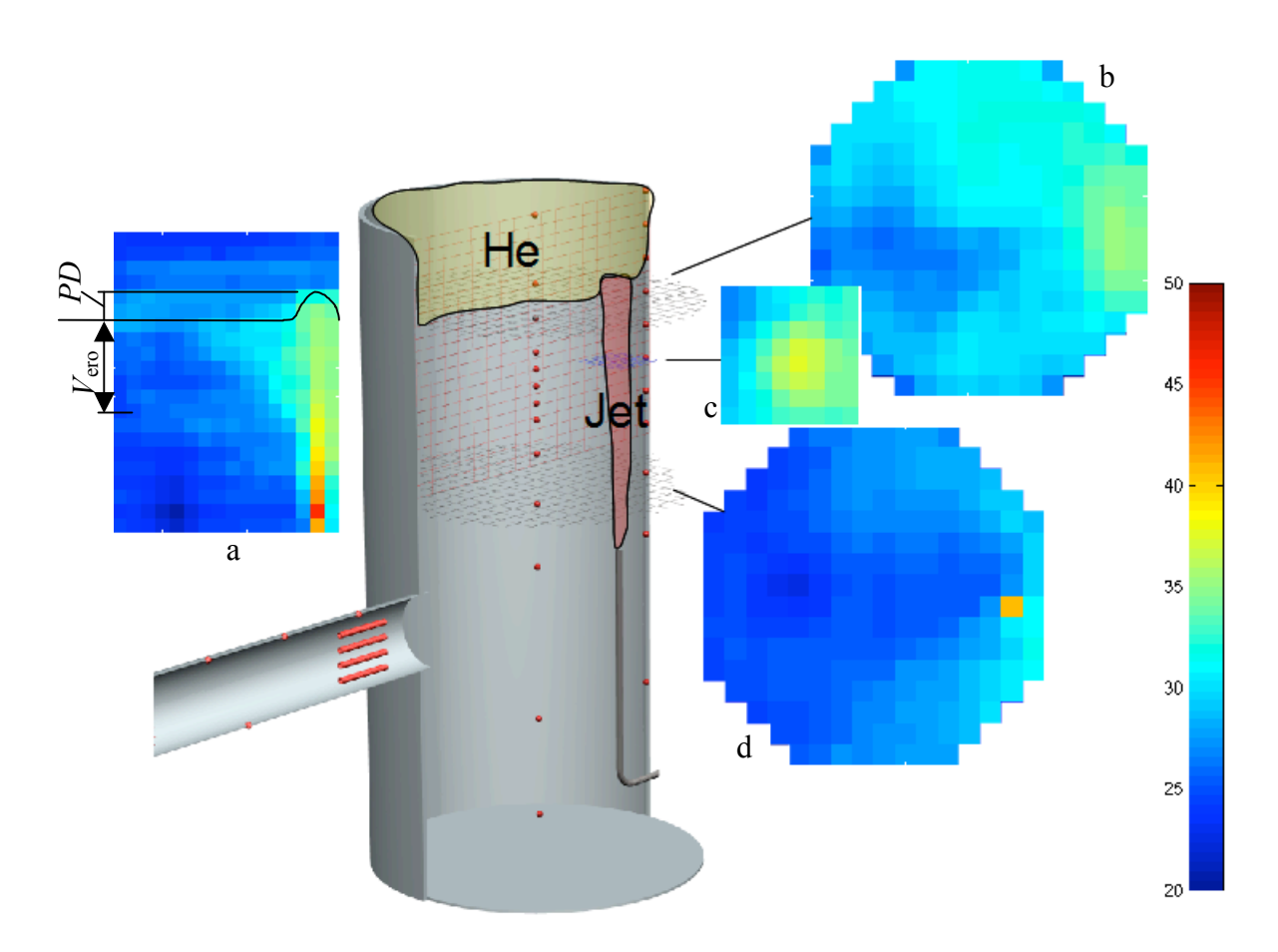


Figure 5: Full display of temperature measurement in Vessel 2 after 2000 s.

Figure 5 displays the temperature field measurements available from Vessel 2 at t=2000 s. From Figure 5, "a", the mushroom-shaped temperature field above the jet can be seen, where the height of the mushroom head equals the penetration depth, PD, of the jet into the layer. The propagation of the erosion front from the initial nominal position to its current position, multiplied by the vessel cross-section, provided the eroded volume, $V_{\rm ero}$ (Figure 5 "a") which was used to quantify and compare the layer erosion process. In Figure 5, "a" and "d", a dark blue zone was identified as a cold pocket in the left part, probably originating from the stratified counter-current flow through the connecting pipe that is set up when helium flushes through it towards the other vessel and a back flow of pure air (later low-helium mixture) is initiated.

From Figure 5, "c", the jet diameter and position can be extracted with the uncertainty originating from the spatial pitch of the temperature measurement matrix. The jet was sucked

towards the right side wall. Figure 5 "b" and "d" exhibit a horse-shoe shaped, asymmetric warm zone (green/yellow) area with an upper smear. After the jet is stopped at the stagnation point it fell down and is pushed aside by the upcoming air.

Considering the temperature evolution at the points of the vertical temperature mesh sensor above the jet (see "d", Figure 1), the propagation of the helium layer erosion front (i.e., the arrival of the stagnation point) is made obvious by an increase in temperature at a certain measurement position (see Figure 6). Thus, V_{ero} can be extracted in a time-dependant way.

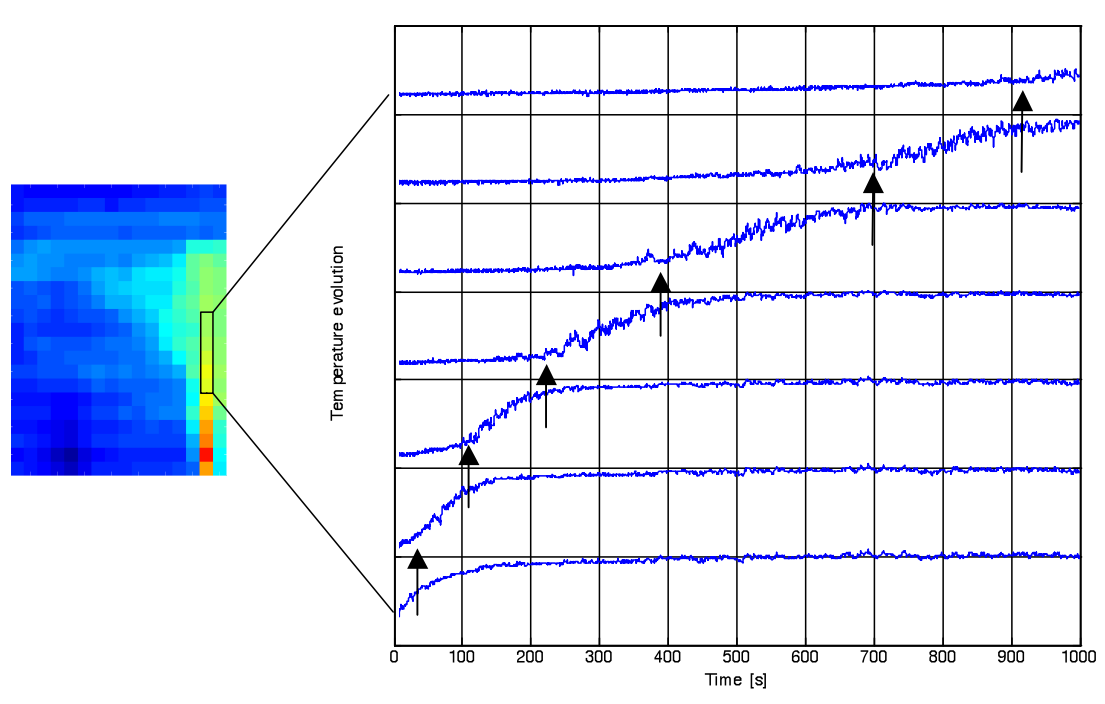


Figure 6: Temperature evolution at selected points from locations above the injected jet (marked in the left graph) with stagnation point arrival times are marked with arrows.

5. Scalability of layer break-up

A geometrically similar experiment with Fr_{int} =0.6 has been carried out at the PANDA facility (PSI) in the frame of the OECD/NEA SETH-2 "Vertical fluid release test series". PANDA is a large-scale test facility where the corresponding drywell vessels are four times larger in size than MiniPanda and have a height of 8 m. In order to compare and quantify the layer erosion process, a non-dimensional volume, V^+ , corresponding to the eroded volume of the layer, was computed Eq. (6)

$$V^{+}(t) = \frac{V_{ero}(t)}{V_{he-laver}},\tag{6}$$

where $V_{\rm ero}$ is the product of the cross-section of the vessel and the distance the temperature front has propagated (see Figure 5) and $V_{\rm he-layer}$ is the initially injected helium layer volume (known from the mass flow controller "Reddy-GSC"). The time axis was normalized with the residence

time, τ_{dil} , of the injected air, i.e. the quotient of the molar amount of helium initially present N_{helium} over the molar injected air flow rate \dot{N}_{air} , a see Eq. (7)

$$\tau_{dil} = \frac{N_{helium}}{N_{air}} \tag{7}$$

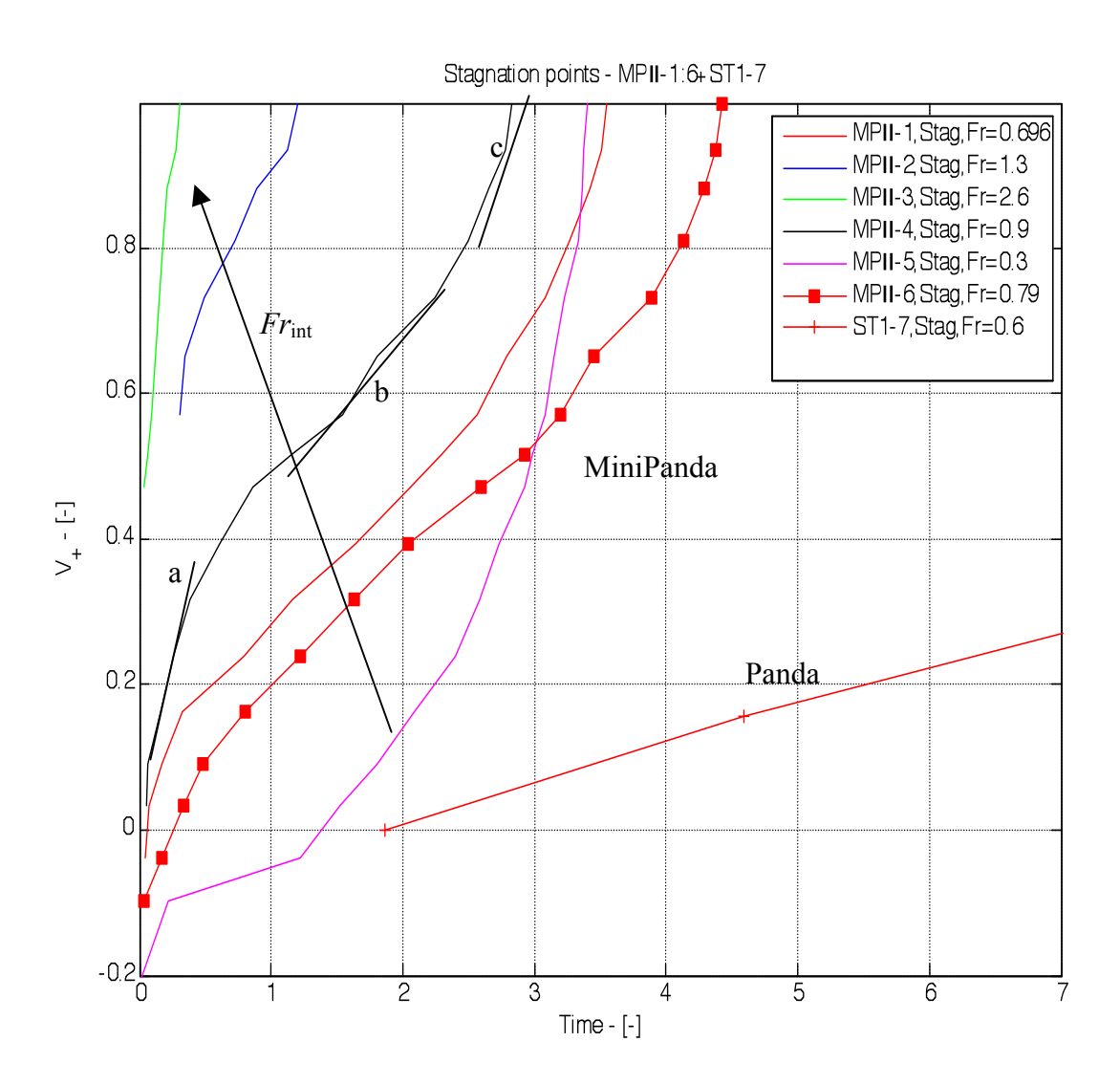


Figure 7: Non-dimensional layer erosion versus non-dimensional time.

Figure 7 displays the layer erosion processes (eroded volume versus scaled time) of experiments conducted at MiniPanda (MPII_1 – MPII_6) with varying Froude number and the ST1_7 experiment conducted at the large-scale facility PANDA. For the MiniPanda experiments MPII_1 to MPII_5 (all experiments with the same initial helium layer concentration), it can be stated, that the erosion accelerates with increasing Froude number. Negative values of the non-

dimensional eroded volume, V+, resulted from the stagnation being stuck already in the transition zone (i.e., low helium fraction zone below the actual height of the nominal initial layer). That's why this negative eroded volume was more expressed for low Froude number experiments where the jet had only a low momentum that was easily dissipated already in the low helium fraction zone.

Usually, the curve was steeper in the beginning (Figure 7, Slope "a") (i.e., the erosion front could propagate faster). Later (Slope "b"), the erosion process slows down (i.e., that curve flattens a bit). Towards the end of the erosion (Slope "c"), the propagation accelerates again (i.e. the curves gets steeper). This is expected to be due to

- 1) reservoir weakening due to diffusion and air entrainment into the layer and thus reducing the helium concentration in the upper part. The diffusion of helium out of the reservoir was supported by the helium concentration jump (i.e., high vertical gradient) that was created at the interface between the reservoir and the well-mixed zone below (see Figure 3, "b" and "c).
- 2) The "lid effect" is also expected to contribute to an acceleration of the erosion towards the end: turbulence induced by the jet-layer-interaction propagated through the layer and had, in the later phase of the experiment, little space to decay. Consequently, the turbulences were reflected at the lid and increased the turbulence-enhanced mixing, resulting in air entrainment, in the remaining helium reservoir.

This "three slope behavior" of the layer erosion velocity could not be observed in the large-scale experiments.

Experiment MPII_6 was intended to further quantify the influence of the diffusion: it was conducted with a similar Froude number as MPII_1 and MPII_4, 0.7 < Fr < 0.9, but the helium reservoir concentration, c_0 , was only 35%. In Figure 7 it can be seen that during experiment MPII_6 the layer was eroded slower than in MPII_1. This is expected to be due to the smaller diffusion contribution for the lower initial helium concentration (τ_{dif} =2930 s for MPII_1 and τ_{dif} =4170 s for MPII_6). Numerically the diffusion effect on the helium reservoir concentration weakening has been compensated for in the helium profile evolution of MPII_1 and MPII_6, resulting in a good matching of the two evolutions on a scaled time axis. This observation supports the hypothesis of a significant influence of the diffusion to the layer break-up process on the small scale experiment.

The very low Froude number experiment MPII_5, conducted with a very low air injection, progressed very slowly on the real time axis. The residence time, τ_{dil} , was consequently large (i.e., τ_{dil} =1422 s) compared to the other experiments and approached the order magnitude of the diffusion time, τ_{dif} =2930 s. Considering the experiments MPII_1-4, all with a higher Froude number, it was expected to reach the end of the erosion for MPII_5 around 6-7 x the residence time, τ_{dil} . This expected time would correspond to 3x the diffusion time, τ_{dif} . The diffusion does not scale with the residence time but superimposed constantly on the air entrainment into the layer (or the reduction of the helium fraction inside the layer). It was not surprising to find, believed due to the relatively larger contribution of the diffusion, that the layer erosion of MPII_5 (Fr=0.3) "overtook" the erosion of MPII_1 (Fr=0.7!) after 2.5x the residence time, τ_{dil} , what equals to 1.5x the diffusion time, τ_{dif} , of MPII_5.

A comparison between MiniPanda (MPII_1, MPII_6) and PANDA (ST1_7), all at about the same Froude number and drawn in red in Figure 7, provides the observation that the large-scale experiment (ST1_7) progresses significantly (about 4 times) slower than the small-scale experiments. This deceleration is expected to originate from

- a) the diffusion length scale that does not decrease for the smaller facility, so that on the four times smaller facility the diffusion is four times stronger for the same initial helium concentration and
- b) the higher air entrainment rate and mixing inside the layer of MiniPanda compared to PANDA.

Two qualitative differences between the large- and the small-scale experiment results caught the author's attention.

- 1) In the large-scale experiments the slope of layer erosion evolution was constant, while during the small-scale experiments a "three slope behavior" of the layer erosion was observed.
- The helium fraction at the top of the facilities: In PANDA, the upper part of the helium reservoir remained unaffected by the processes at the interface for the first $3.7 \cdot \tau_{dil}$ (Studer, Brinster et al. 2010). There, the helium fraction evolution was in-line with the pure diffusion helium fraction decrease at the beginning of the experiment. In MiniPanda, the jet experiment's helium concentration evolution deviated after $0.5 \cdot \tau_{dil}$ from the diffusion.

In the large- as well in the small-scale experiment results, the deviation between the helium concentration of the test with and without air injection occurred later for measurement positions at higher levels, indicating that the limit between a pure molecular process and another mixing process is moving upward with time.

At this point, the Reynolds number of the jet at the exit should be discussed: For the PANDA experiment, Re_{PANDA} is around 14000. In order to obtain a high $Re_{MiniPanda}$ at low Froude numbers, the density ratio was set to maximum (i.e., a 100% helium layer in an air environment) and a $Re_{MiniPanda}$ of 2350 was achieved at Fr_{int} =0.7. As discussed, this high concentration leads to a strong superimposed diffusion. The diffusion was reduced in experiment MPII_6, but then the $Re_{MiniPanda}$ decreased to 1250, one order of magnitude less than in PANDA. In order to keep Froude and Reynolds number constant on both scales, where also the vertical jet exit diameter is exactly scaled, one would have to conduct a MiniPanda experiment with a very large environment gas density (air density). But, for very large gas densities, the Froude number converges to unity (see Eq. (3)). Consequently, for a linear scaling, Froude and Reynolds number cannot be kept equal for both scales at the same time.

Further investigation is needed in order to clarify why the air entrainment into the stratified layer is so much higher for MiniPanda compared to PANDA, even though the Reynolds number for MiniPanda is so much lower. In addition, the diffusion should be considered in the time scaling with a correction factor.

6. Conclusion

In the present contribution, the erosion and break-up of a stratified layer are observed experimentally. The small(/smart)-scale facility MiniPanda, with its novel instrumentation, enables a thorough understanding of the process and provides CFD-grade measurement data with a spatial resolution in the order of magnitude of the computational meshes.

A comparison between geometrically similar experiments on two different length scales reveals the importance of the diffusion-, and other physical processes that do not scale with the facility size. In fact, the negligence of transport components such as diffusion and turbulence enhanced mixing lead to an erroneous over-estimation of the layer break-up velocity of a stratified layer. For the same boundary conditions, the helium layer in the large-scale experiment was much more stable and it needs to be questioned if a true containment layer is even more stable, and how much more so.

In the next step, analytical investigations of the layer break-up phenomena on both scales, with the state-of-the-art CFD codes CFX, StarCCM+ and Fluent, and a comparison with the experimental data, will answer the question of, if, and how precise, the codes are able to predict the process and if they can provide further understanding why the processe on the two scales behaved differently.

7. References

Allelein, H. J., K. Fischer, et al. (2007). "International Standard Problem ISP-47 on Containment Thermal-hydraulics." <u>NEA News 2007</u> **25.2**.

D'Auria, F. and G. M. Galassi (2010). "Scaling in nuclear reactor system thermal-hydraulics." <u>Nuclear Engineering and Design</u> **240**(10): 3267-3293.

Dreier, J., D. Paladino, et al. (2008). <u>PANDA: a Large Scale Multi-Purpose, Test Facility for LWR Safety Research</u>. PHYSOR08, Interlaken, Switzerland.

Fischer, K., L. Wolf, et al. (2002). Scaling of containment experiments -SCACEX-. <u>5th Euratom Framework Programme</u>.

Karwat, H. (1987). "Scaling and extrapolation of hydrogen distribution experiments." <u>Nuclear Engineering and Design</u> **104**(3): 285-294.

Peterson, P. F. (1994). "Scaling and analysis of mixing in large stratified volumes." <u>International Journal of Heat and Mass Transfer</u> **37**(Supplement 1): 97-106.

Peterson, P. F., V. E. Schrock, et al. (1998). "Scaling for integral simulation of mixing in large, stratified volumes." <u>Nuclear Engineering and Design</u> **186**(1-2): 213-224.

Prasser, H. M., A. Böttger, et al. (1998). "A new electrode-mesh tomograph for gas-liquid flows." Flow Measurement and Instrumentation 9(2): 111-119.

Revankar, S. T., S. Oh, et al. (2009). "Scaling of passive condenser system for separate effect testing." <u>Nuclear Engineering and Design</u> **239**(10): 1870-1878.

Ritterath, M., H.-M. Prasser, et al. (2010). "New gas concentration measurement system for the PANDA containment test facility." <u>Nuclear Engineering and Design</u> **in press**.

Ritterath, M., P. Voser, et al. (2009). <u>Robust Thermal Flow Sensor for a Containment Test Facility</u>. IEEE Sensors, Christchurch, New Zealand, IEEE.

Schlichting (1960). Boundary Layer Theory. MGraw Hill.

Studer, E., J. Brinster, et al. (2010). <u>Interaction of a light gas stratified layer wiith an air jet coming from below: Large scale experiments and scaling issues</u>. XCFD4NRS, Washington.

VDI (2008). VDI-Wärmeatlas. Düsseldorf, VDI Gesellschaft.

Wulff, W. (1996). "Scaling of thermohydraulic systems." <u>Nuclear Engineering and Design</u> **163**(3): 359-395.

Yadigaroglu, G., M. Andreani, et al. (2003). "Trends and needs in experimentation and numerical simulation for LWR safety." <u>Nuclear Engineering and Design</u> **221**(1-3): 205-223.

Zuber, N., G. E. Wilson, et al. (1998). "An integrated structure and scaling methodology for severe accident technical issue resolution: Development of methodology." <u>Nuclear Engineering and Design</u> **186**(1-2): 1-21.